STUDY OF STRUCTURAL AND MAGNETIC PROPERTIES OF $Co_{1-x}Zn_xCr_{0.5}Fe_{1.5}O_4$ FERRITE THIN FILM BY PLD TECHNIQUE

T. ZEESHAN*, S. ANJUM , S. WASEEM, R. ZIA
Department of physics, Lahore College for Women University, Lahore, Pakistan 54000.

The Zinc doped cobalt chromium ferrites with the general formula $Co_{1-x}Zn_xCr_{0.5}Fe_{1.5}O_4$ are used to deposit the thin films on silicon Si (100) substrate using pulsed laser deposition technique keeping the substrate temperature constant at 450^oC. The pressure inside the chamber was 10^{-4}Torr. After deposition these thin films have been post annealed at $800C^0$ to achieve the crystallinity. The structural properties, surface analysis, magnetic and optical properties have been analyzed by X-ray Diffractrometer, Atomic Force Microscopy, Spectroscopy Ellipsometry and Vibrating Sample Magnetometer respectively. XRD analysis revealed that lattice parameters decreases from 8.796 A^0 to 8.705 A^0 and crystallite size increases from 19 nm to 68nm with increasing the zinc contents. AFM analysis showed that average roughness increases with enhancement of zinc which may be due to increasing grain size and thickness. The ellipsometric analysis revealed that the band gap energy increases from 1.91 eV to 3.0 eV.

(Received November 16, 2017; Accepted January 20, 2018)

Keywords: Refractive index, Grain size, Thin films, Band gap energy

1. Introduction

Recently the research in material science is concentrated on invention of novel materials with enhanced properties to overcome the new technological demands. The main advantages of ferrites are that they produce high efficiency, suitable dielectric loss, low cost, hence find the prospective application in memory cores and memory devices[1] . Several groups studied the effect of substitutions with diverse cations to enhance the properties of spinel ferrites. Among the spinel ferrites, the most extensively studied ferrites are the cobalt ferrites because it has unique magnetic properties, for example high resistivity, chemical stability, moderate saturation magnetization and positive anisotropic constant. Now a days, thin films of cobalt ferrites, doped cobalt ferrites and their composites have been used as a potential components for the application of gas sensors [2][3]. The thin films of cobalt ferrites can be attained by various techniques but the best favorable technique for the growth of epitaxial thin films with perpendicular magnetic anisotropy and a privileged crystallographic direction was found to be Pulsed Laser Deposition(PLD) [4, 5]. The lasers with pulse duration of nanosecond e.g. Nd-YAG have been used for the growth of film. Thin films of soft magnetic material like Mn-Zn or Ni-Zn with high ac permeability and high resistivity can be used in micro transformer, micro inductor and magnetic recording.

Fujiwara et al. reported the influence of zinc contents on electric resistivity and permeability of $Zn_xFe_{3-x}O_4$ ferrite thin films [6]. The permeability and natural resonance frequency can be modified by adjusting the zinc concentration [7].

Matsushita et al. studied the cobalt doped nickel zinc ferrite thin films deposited by spin spray technique have high permeability and high resonance frequency exceeding snoek's limit for sintered bulk ferrites [8].

The aim of present work is to study the structural, optical and magnetic properties of zinc doped cobalt chromium ferrite thin films.

*Corresponding author: talats@hotmail.com

2. Experimental theory

Thin films of $Zn_xCo_{1-x}Cr_{0.5}Fe_{1.5}O_4$ magnetic materials with different composition were deposited on Si (100) substrate. A schematic diagram of the experimental setup is shown in Fig. 1.

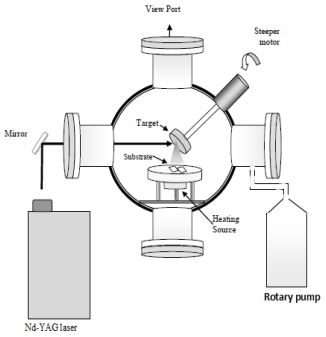

Fig 1: A schematic of the experimental setup for PLD

The ablation of each target was done by Nd-YAG laser with wave length of 248 nm at a fluence of 2.5 J/cm^2 and operated at a repetition rate of 20 Hz. The base pressure in the chamber was ~ 10^{-4}Torr which was attained by rotary pump. An optimized distance between substrate and target is 1.5cm. The rotation of target was done by using a programmable motor mounted at 6 rpm. The irradiation of each target was done with 5000 number of shots and the substrate temperature is also kept constant in each case i.e. 300K. After deposition, the thin films have been annealed at 850 ^{0}C to achieve the crystallinity. Finally the prepared thin films have been characterized by the following techniques.

3. XRD analysis

The comparative XRD patterns of $Zn_xCo_{1-x}Cr_{0.5}Fe_{1.5}O_4$ where (x=0, 0.2, 0.4, 0.6, 0.8, 1.0) thin films are shown in figure 1. It is observed from the XRD patterns that all the films exhibit single phase cubic spinel structure having two prominent peaks in the direction of (220) and (311). All the thin films have the preferential plane in the direction of (220) direction. All other peaks of spinel structure are not observed in these micrographs because XRD measurement has been taken out of plane which detects only those planes that existed perpendicular to the surface of sample.
It is noted that the (311) peak is not grown in the thin films at x=0 to 0.6 because in these samples all the peaks are grown parallel to the surface of the thin films but as the concentration of zinc increases, the (311) plane starts to grow in the direction perpendicular to the surface of thin films.

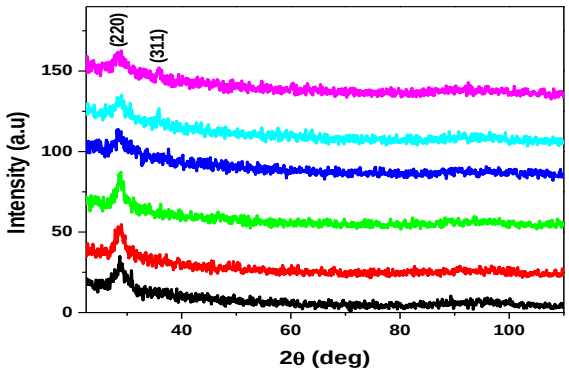

Fig. 2. Comparative XRD patterns of $Co_{1-x}Zn_xCr_{0.5}Fe_{1.5}O_4$ thin films

The d spacing of the zinc doped ferrites has been calculated by using the Bragg's law

$$n\lambda=2d\sin\theta \quad (1)$$

Where, λ is the wave length of Cu- kα having value 1.54A^{o}. The lattice parameters have been calculated using the following relations [9]:

$$a= d\ (h^2+k^2+l^2) \quad (2)$$

Where h, k, l are the miller indices. To calculate the crystallite size along (220) plane Scherrer's formula is employed [10]

$$D_P= 0.9\lambda/\beta\cos\theta \quad (3)$$

Where D_P is the crystallite size, β is the full width at half maximum and θ is the peak position. The parameters extracted from the XRD pattern are listed in the table 1.

It has been observed from the table that lattice parameter "*a"* decreases as the concentration of Zinc increases. We can explain the reduction of lattice parameter in to two regimes.

As the ionic radius of zinc (0.82 A°) is larger than cobalt (0.78 A°), so during heating of the substrate thermal expansion induces the lattice mismatch which causes the decrease in the lattice parameters.

It is revealed that the most preferential intense peak (220) in the spectra is slightly shifted towards the lower angle which overcomes the interfacial stresses and strains between the surface of the substrate and thin film, which causes to reduce the lattice parameters [11].

Table 1. Parameters extracted from XRD pattern

Zinc content (x)	**2θ (deg.)**	**d-spacing (nm)**	**FWHM (Rad.)**	**Lattice parameters (A^0)**	**Crystallite size(nm)**
$Co_{1-x}\ Zn_0Cr_{0.5}\ Fe_{1.5}\ O_4$	28.6804	3.1100	0.3545	8.496	19
$Co_{1-x}\ Zn_{0.2}Cr_{0.5}\ Fe_{1.5}\ O_4$	28.6932	3.1087	0.2960	8.492	22
$Co_{1-x}\ Zn_{x0.4}Cr_{0.5}\ Fe_{1.5}\ O_4$	28.8241	3.0948	0.1256	8.453	26
$Co_{1-x}\ Zn_{0.6}Cr_{0.5}\ Fe_{1.5}\ O_4$	28.8784	3.0891	0.1286	8.437	36
$Co_{1-x}\ Zn_{0,8}Cr_{0.5}\ Fe_{1.5}\ O_4$	28.9854	3.0780	0.1503	8.405	40
$Co_{1-x}\ Zn_{1.0}Cr_{0.5}\ Fe_{1.5}\ O_4$	28.9328	3.0835	0.0624	8.421	68

It has been observed from Table 1 that the crystallite size increases with increasing the zinc contents. It is well known that the lattice mismatch between the substrate and the film produces the stresses during the deposition and these stresses also significantly affect the properties and structure of film. It has been seen from the table that the lattice parameter decreases that's why the strains in the films reduce and the crystallite size increases.

It has already been discussed that the structure achieved in the thin films are cubic spinel, and this cubic structure consist of two sites tetrahedral and octahedral. The distance between the magnetic ions in tetrahedral and octahedral sites are L_A and L_B respectively and they are calculated by the relation (4) and (5).

$$L_{A=}\frac{a\sqrt{3}}{4} \quad (4)$$

$$L_{B=}\frac{a\sqrt{2}}{4} \quad (5)$$

The values calculated for the hopping lengths L_A and L_B are given in table 2.

It is observed from the table that the hopping lengths of the ions decrease with increasing the zinc concentration. As L_A and L_B are directly proportional to the lattice constant, so by increasing zinc the concentration the lattice constant decreases which lead to decrease in L_A and L_B. The variation of hopping length with zinc contents has been shown in Fig. 3.

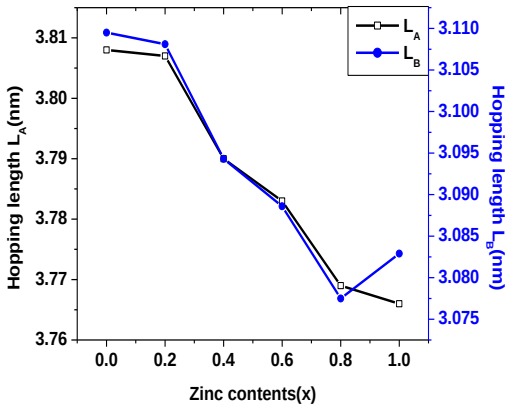

Fig. 3.Correlation of hopping lengths with zinc contents.

Table 2. Variation of hopping lengths with zinc

Zinc content (x)	**L_A (nm)**	**L_B (nm)**
$Co_{1-x}\ Zn_0Cr_{0.5}\ Fe_{1.5}\ O_4$	3.808	3.1095
$Co_{1-x}\ Zn_{0.2}Cr_{0.5}\ Fe_{1.5}\ O_4$	3.807	3.1081
$Co_{1-x}\ Zn_{x0.4}Cr_{0.5}\ Fe_{1.5}\ O_4$	3.790	3.0943
$Co_{1-x}\ Zn_{0.6}Cr_{0.5}\ Fe_{1.5}\ O_4$	3.783	3.0886
$Co_{1-x}\ Zn_{0,8}Cr_{0.5}\ Fe_{1.5}\ O_4$	3.769	3.0775
$Co_{1-x}\ Zn_{1.0}Cr_{0.5}\ Fe_{1.5}\ O_4$	3.766	3.0829

4. AFM analysis

The AFM images of deposited thin films have been shown in figure 4. The calculated values from 2-dimentional and 3-dimentional images of the AFM are the means grain size and average roughness which have been summarized in table 3.

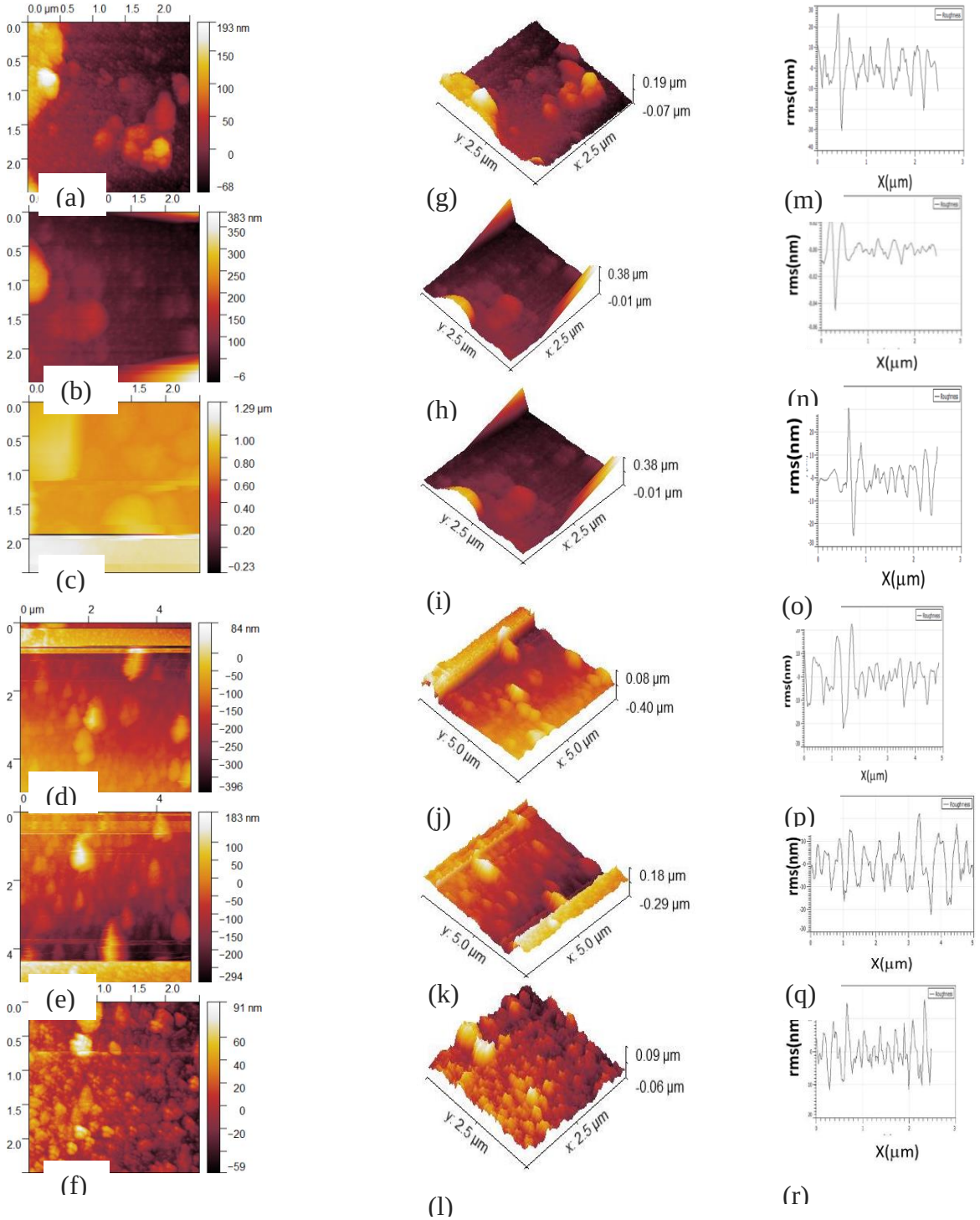

Fig. 4.AFM analysis of zinc doped cobalt chromium ferrites, analysis, 2D (a, b, c, d, e, f), 3D(g, h, i, j, h, l) and line profile of roughness(m, n, o, p, q, r)

The figure (a, b, c, d) showing the smooth surface but the figure (e, f) that have larger concentrations of zinc, the granular structure has been observed. The average grain size calculated from the AFM analysis is showing the similar trend as the crystallite size. It has been observed from the table that the average roughness increases with increase in the concentration of Zinc. The average roughness increases due to increase in thickness and the grain size [12] which is shown in figure 5. The roughness calculated from the ellipsometric analysis and AFM are approximately comparable.

Table 3: Average roughness and grain size calculated from AFM

Zn contents (x)	Average roughness (nm)	Grain size (nm)
$Co_{1-x}Zn_0Cr_{0.5}Fe_{1.5}O_4$	4.0	646
$Co_{1-x}Zn_{0.2}Cr_{0.5}Fe_{1.5}O_4$	5.0	737
$Co_{1-x}Zn_{0.4}Cr_{0.5}Fe_{1.5}O_4$	5.6	734
$Co_{1-x}Zn_{0.6}Cr_{0.5}Fe_{1.5}O_4$	6.7	847
$Co_{1-x}Zn_{0.8}Cr_{0.5}Fe_{1.5}O_4$	5.6	556
$Co_{1-x}Zn_{1.0}Cr_{0.5}Fe_{1.5}O_4$	7.1	876

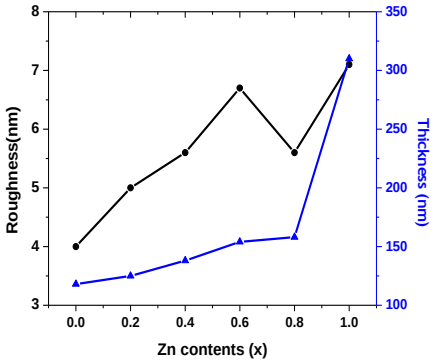

Fig. 5.Graph between thickness and roughness

5. Ellipsometry analysis

The optical parameters like absorption, refraction, refractive index, optical band gap energy, thickness and roughness are determined by Spectroscopy Ellipsometry. The refractive index of all deposited films has been shown in the figure 6.

It has been observed from the figure that the refractive index is high in the region of 500-600 nm and the refractive index decreases with enhancement of zinc ions. This decreasing trend of "n" is due to increase in thickness and roughness of the film.

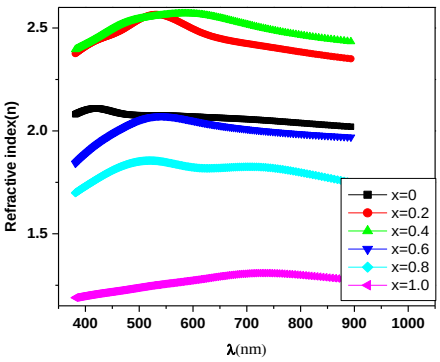

Fig .6.Variation of refractive index with different concentration of zinc

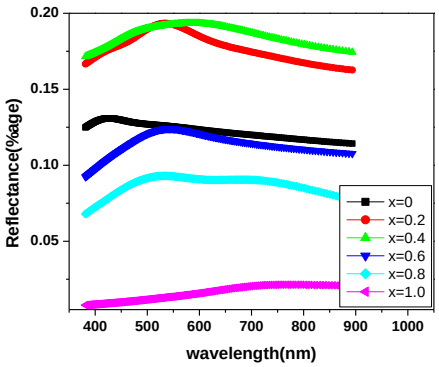

Fig. 7.Comparison of reflectance with different concentration of zinc

It has been observed from the figure 7 that value of reflectance is maximum for x=0.2 and x=0.4 and then its value decreases for higher concentration of zinc. This behavior can be attributed to the less reflecting nature of zinc and increase in thickness.

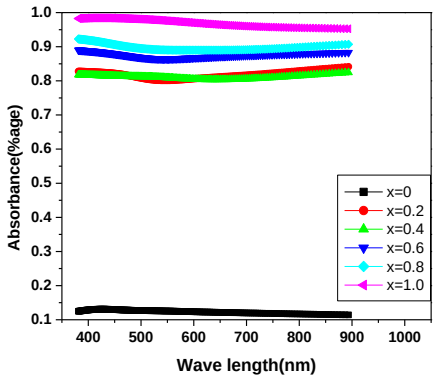

Fig. 8.Comparison of absorbance with different concentration of zinc

The figure 8 shows that the absorbance increases with increasing the zinc contents. The higher value of absorbance with greater concentration of zinc is due to highly absorbing nature of zinc and increased thickness of the films. The both AFM analysis and ellipsometric analysis shows that the roughness and thickness are increasing with increasing the zinc contents which is also responsible for increasing absorbance.

The optical band gap energy can be calculated by using the following relation[13].

$$(\alpha h\upsilon)^2 = A\,(h\upsilon - E_g)^m \qquad (6)$$

Where "A" is constant and its value is different for different materials. The $(\alpha h\upsilon)^2$ is plotted verses $(h\upsilon)$ which has been shown in figure 9 (a, b, c). The band gap energy is calculated by extra plotting the linear part to $(\alpha h\upsilon)^2 = 0$

It has been analyzed that at x=0 where the zinc contents is absent, the band gap energy is minimum. It has been noticed that there is significant decrease in band gap energy with the doping of zinc from x=0.2 to x= 0.8 which is due to increase in crystallite size and film thickness. The relationship between crystallite size and energy band gap has been drawn in figure 10. As the crystallite size increases the valance and conduction bands become closer and narrowing the band gap. Moreover at x=1.0 where the zinc content is maximum and cobalt is absent the band gap energy increases again. As increase in thickness results the uniform and homogenous network of defects results an increase in band gap. [14].

It has been analyzed from the data listed in table that film thickness increases from 118 to 310nm with the enrichment of zinc contents. The increase in thickness is due to reduced stresses at the interface of substrate and thin film or may be due to adhesion forces between the deposited materials and the substrate [15]. It is noted that the surface roughness increases with increasing the zinc ions and its values are in accordance with AFM results.

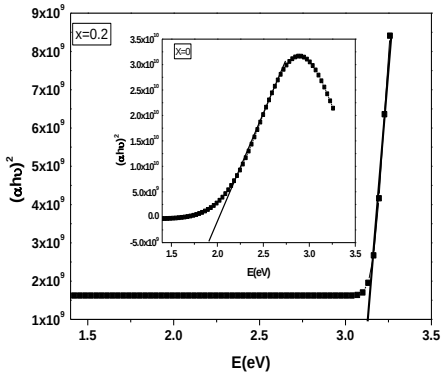

Fig. 9(a). Optical band gap energy of $Co_{1-x}Zn_xCr_{0.5}Fe_{1.5}O_4$ thin films at x=0 and 0.2

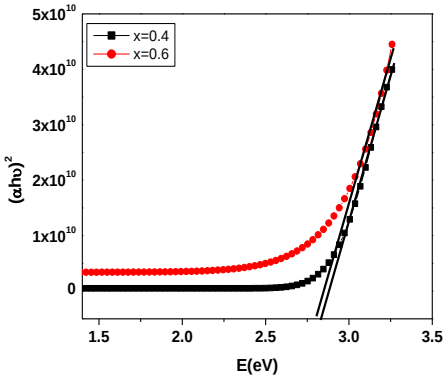

Fig. 9(b). Optical band gap energy of $Co_{1-x}Zn_xCr_{0.5}Fe_{1.5}O_4$ thin films at x=0.4 and 0.6

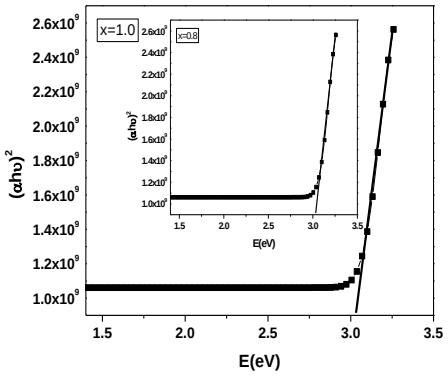

Fig. 9(c).Optical band gap energy of $Co_{1-x}Zn_xCr_{0.5}Fe_{1.5}O_4$ thin films at x=0.8 and 1.0

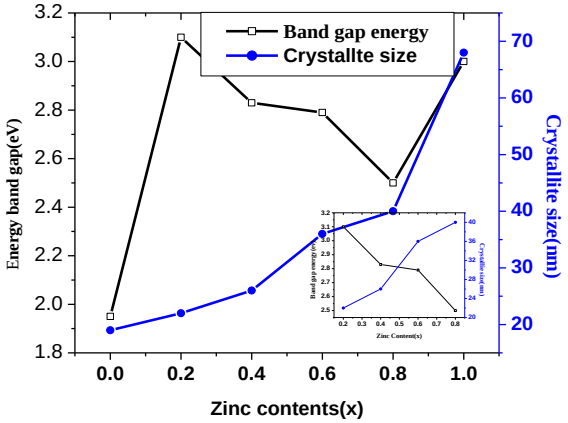

Fig 10: Variation of band gap energy and crystallite size with zinc content in $Co_{1-x}Zn_xCr_{0.5}Fe_{1.5}O_4$ thin films:(inset) is the variations from x=0.2 to x=0.4

Table 4: Thickness, roughness, optical band gap and refractive index

Zinc content (x)	Thickness (nm)	Roughness (nm)	Optical band gap (eV)	Refractive index (n)
$Co_{1-x}Zn_0Cr_{0.5}Fe_{1.5}O_4$	118	15	1.95	2.1
$Co_{1-x}Zn_{0.2}Cr_{0.5}Fe_{1.5}O_4$	125	19	3.1	2.57
$Co_{1-x}Zn_{0.4}Cr_{0.5}Fe_{1.5}O_4$	138	20	2.83	2.55
$Co_{1-x}Zn_{0.6}Cr_{0.5}Fe_{1.5}O_4$	154	25	2.79	2.0
$Co_{1-x}Zn_{0,8}Cr_{0.5}Fe_{1.5}O_4$	158	20	2.5	18
$Co_{1-x}Zn_{1.0}Cr_{0.5}Fe_{1.5}O_4$	310	35	3.0	1.2

6. Magnetic properties

The hysteresis loop of thin films recorded at room temperature using vibrating sample magnetometer is shown in Fig. 11. The magnetic properties of thin films depends on the grain size, surface morphology and magnetic anisotropy of the ferrite films [16].

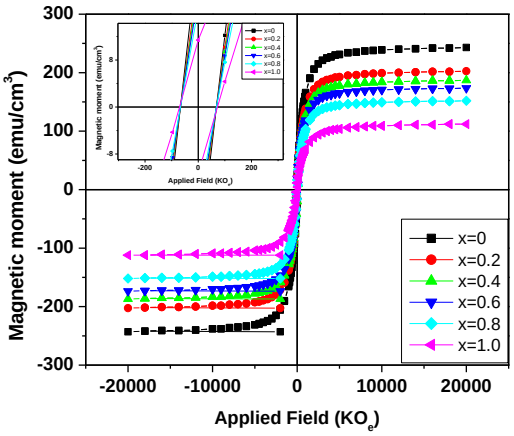

Fig.11 .Hysteresis loop of $Co_{1-x}Zn_xCr_{0.5}Fe_{1.5}O_4$ thin films

The values of saturation magnetization, Remnant magnetization and coercivity of the deposited thin films are listed in the table 4.

Table 5: Parameters extracted from M-H loop of $Co_{1-x}Zn_xCr_{0.5}Fe_{1.5}O_4$ thin films

Zn concentration (x)	Saturation magnetization(emu/g)	Remnant magnetization (emu/g)	Coercivity (K Oe)
$Co_{1-x}Zn_0Cr_{0.5}Fe_{1.5}O_4$	220	27	73
$Co_{1-x}Zn_{0.2}Cr_{0.5}Fe_{1.5}O_4$	243	24	70
$Co_{1-x}Zn_{0.4}Cr_{0.5}Fe_{1.5}O_4$	203	21	69
$Co_{1-x}Zn_{0.6}Cr_{0.5}Fe_{1.5}O_4$	186	20	66
$Co_{1-x}Zn_{0.8}Cr_{0.5}Fe_{1.5}O_4$	160	18	65
$Co_{1-x}Zn_{1.0}Cr_{0.5}Fe_{1.5}O_4$	110	11	68

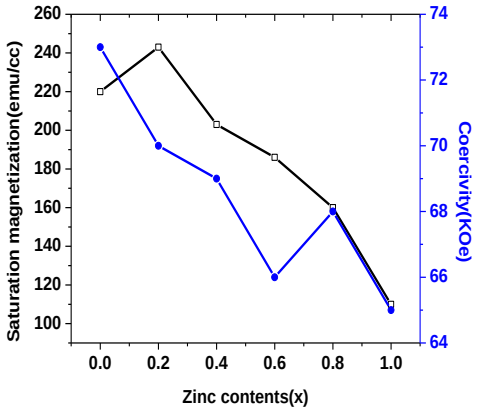

Fig. 12. Variation of saturation magnetization and coercivity with zinc

Both the saturation magnetization and coercivity decreases with increasing the zinc contents which is shown in figure 12.

The decrease in saturation magnetization with increasing the zinc contents is due to non-magnetic nature of zinc. The deviation in magnetic properties of this kind of spinel ferrites can be clarified by the distribution of cations and the change in interaction between "A" and "B" sites. When the zinc concentration is low the magnetic moment of the ions at (A site) is antiparallel to magnetic moment at (B- site) due to supper exchange interaction. The net magnetic moment can be explained by using the relation

$$M = M_B - M_A \tag{7}$$

It is well known that the zinc prefers to occupy the A-site and cobalt prefers to occupy the B-site and iron is equally distributed between A and B sites. The replacement of iron ions (Fe^{3+}) by the zinc ions (Zn^{+2}) will decrease the (M_A) magnetic moment which leads to increase the net magnetic moment. However, by increasing the zinc contents the net magnetization can be explained as given below

$$M_B \cos\alpha_{\gamma k} - M_A \tag{8}$$

Where $\alpha_{\gamma k}$ is the Yafet-kittle angle or canting angle between the moments at B-site that has a relation with non-magnetic nearest neighbor ions at the B site[17].

For x<=0.4 the magnetic moment of the remaining iron ions in site A is no more able to align the magnetic moment of ions at the B-site antiparallel .The lattice at the B-site then divides itself into sub-lattices and their magnetic moments establishes the canting angles with each other[18]. Hence more replacement of the zinc ions with iron ions causes to decrease in magnetic moment at B site and consequently decrease in saturation magnetization. The magnetic properties

are also affected by thickness of the film so the decrease in coercivity with increasing the zinc contents is also due to increasing thickness. As the thickness increases, the size of grains increases which leads to decrease in grain boundaries that causes to decrease in coercivity[19]. It has been observed that both coercivity and saturation magnetization have greater values as compare to the reported values of bulk . The microstructure of the thin film has great influence on the coercivity values. In case of thin film, the grain boundaries increase due to smaller grain than the bulk materials. These grain boundaries behave like pinning sites for the domain wall which are responsible for the high coercivity values [19, 20].

Conclusions

$Co_{1-x}Zn_xCr_{0.5}Fe_{1.5}O_4$ thin films have been successfully prepared by PLD techniques. The lattice parameters have been decreased and crystallite size increases with increasing the zinc concentration that may be due to the internal stresses. The AFM analysis determined that the roughness increases which may be due to the increasing thickness and the crystallite size. The ellipsometric data showed that the absorbance is maximum and reflectance is minimum which is due less reflecting nature of zinc and increasing thickness. The band gap energy decreases from x=0.2 to 0.8 that is attributed to increasing crystallite size. The magnetic measurements showed that saturation magnetization decrease from 220 to 110emu/g and coercivity decreases from 73 to 68 KOe which is appropriate for magneto-opto electronic recording devices.

References

[1] I. Soibam, S. Phanjoubam, H. Sharma, H. Sarma, R. Laishram, C. Prakash, Solid State Commun **148**(9),399 (2008).
[2] N. Rezlescu, C. Doroftei, E. Rezlescu, P. Popa, Sens. Actuators, B **133**(2),420(2008).
[3] C. Xiangfeng, L. Xingqin, M. Guangyao, Sens. Actuators, B **55**(1),19(1999).
[4] P. Dorsey, P. Lubitz, D. Chrisey, J. Horwitz, J. Appl. Phys **79**(8),6338(1996).
[5] J.L. M. Ning, C.K. Ong, S. J. Wang, Appl. Phys. Express **103**(1),013911(2008).
[6] T. Kiyomura, Y. Maruo, M. Gomi, J. Appl. Phys **88**(8),4768(2000).
[7] A. Fujiwara, M. Tada, T. Nakagawa, M. Abe, J.Magn.Magn.Mater **320**(8) L67(2008).
[8] N. Matsushita, T. Nakamura, M. Abe, Appl. Phys. Express **39**(5),3127(2003).
[9] M.S. Dresselhaus, G. Dresselhaus, P.C. Eklund, Science of fullerenes and carbon nanotubes: their properties and applications, 1st ed., Academic press, USA, 1996.
[10] B. Cullity, Elements of X-ray Diffraction. Addison and Wesley Publishing Company Inc, 2nd ed., Jhon Willy and sons, USA, 1978.
[11] J.L.H. Chau, M.-C. Yang, T. Nakamura, S. Sato, C.-C. Yang, C.-W. Cheng, Optics & Laser Technology **42**(8), 1337 (2010).
[12] J. Islam, Y. Yamamoto, H. Hori, J. Magn. Magn. Mater, **310**(8),2234(2007).
[13] S. Anjum, M.S. Rafique, M. Khaleeq-ur-Rahman, K. Siraj, A. Usman, S. Hussain, S. Naseem, J. Magn. Magn. Mater **324**(2),711(2012).
[14] A. Iqbal, A. Mahmood, T.M. Khan, E. Ahmed, Prog. Nat. Sci **23**(5), 64(2005).
[15] J. Tauc, R. Grigorovici, A. Vancu, Phys. Status Solidi **15**(5),627(1966).
[16] Y.-P. Zhao, R. Gamache, G.-C. Wang, T.-M. Lu, G. Palasantzas, J.T.M. De Hosson, J. Appl. Phys **89**(1),1325(2001).
[17] A. Raghavender, D. Pajic, K. Zadro, T. Milekovic, P.V. Rao, K. Jadhav, D. Ravinder, J. Magn. Magn. Mater **316**(2), 1 (2007).
[18] J. Smit, H. Wijn, Ferrites 2nd ed., Jhon Willy and sons, NewYork, USA, 1959.
[19] N. Gupta, A. Verma, S.C. Kashyap, D. Dube, J. Magn. Magn. Mater **308**(1), 137(2007).
[20] Y. Yamamoto, H. Tanaka, T. Kawai, J. Magn. Magn. Mater **261**(2), 263 (2003).